# Self-Assembly and Thermal Stability of Binary Superlattices of Gold and Silicon Nanocrystals

**ARTICLE** *in* JOURNAL OF PHYSICAL CHEMISTRY LETTERS · OCTOBER 2013

Impact Factor: 7.46 · DOI: 10.1021/jz401964s · Source: PubMed



**4 AUTHORS**, INCLUDING:

Yixuan Yu
University of Texas at Austin
**18** PUBLICATIONS **114** CITATIONS
SEE PROFILE

D.-M. Smilgies
Cornell University
**262** PUBLICATIONS **5,526** CITATIONS
SEE PROFILE

THE JOURNAL OF PHYSICAL CHEMISTRY Letters

Letter

pubs.acs.org/JPCL

# Self-Assembly and Thermal Stability of Binary Superlattices of Gold and Silicon Nanocrystals

Yixuan Yu,[†] Christian A. Bosoy,[†] Detlef-M. Smilgies,[‡] and Brian A. Korgel*,[†]

[†]Department of Chemical Engineering, Texas Materials Institute and Center for Nano- and Molecular Science and Technology, The University of Texas at Austin, Austin, Texas 78712-1062, United States

[‡]Cornell High Energy Synchrotron Source (CHESS), Cornell University, Ithaca, New York 14853, United States

Supporting Information

**ABSTRACT:** Simple hexagonal (sh) $AB_2$ binary superlattices (BSLs) of organic ligand-capped silicon (A; 5.40(±9.8%) nm diameter) and gold (B; 1.88(±10.1%) nm diameter) nanocrystals were assembled by evaporation of colloidal dispersions and characterized using transmission electron microscopy (TEM) and grazing incidence small-angle X-ray scattering (GISAXS). When deposited on tilted substrates by slow evaporation, the sh-$AB_2$ superlattice contracted slightly toward the substrate with centered orthorhombic structure. Heating the BSL to 200 °C in air led to gold coalescence and segregation to the surface of the assembly without disrupting the Si nanocrystal sublattice, thus creating a sh superlattice of Si nanocrystals.

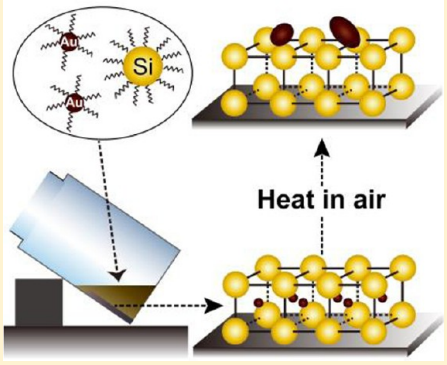


**SECTION:** Glasses, Colloids, Polymers, and Soft Matter

Nanocrystal superlattices and their self-assembly have been widely studied as experimental models to gain deeper understanding about ordering processes that occur in nature and as a route to new materials with unique and synthetically tunable properties.[1−12] Nanocrystals can be made with a tremendous range of composition, size, shape, and surface chemistry, enabling wide tunability of material properties and the interparticle interactions involved in the assembly process. Binary nanocrystal superlattices in particular represent an interesting class of these materials. Self-assembly of nanocrystals with two distinct sizes can yield mesoscopic composition profiles that cannot be obtained any other way, and binary superlattices (BSLs) have been made with metals,[13−15] semiconductors,[16−18] and magnets.[3,13,14,19] Recently, ternary nanocrystal superlattices have been made by matching nanocrystals with three distinct sizes.[20−22] Nonetheless, BSLs containing one of the most commercially important semiconductors, silicon (Si), have not yet been made. BSL formation requires nanocrystals with uniform size and shape and appropriate size matching between two nanocrystal components, and only recently have sterically stabilized Si nanocrystals been made with sufficiently narrow size distributions to form superlattices.[23] Here, we take these highly uniform Si nanocrystals and form BSLs. Si nanocrystals (5.4 nm diameter) were combined with Au nanocrystals (1.9 nm diameter)—both capped with dodecyl ligands—to form BSLs with simple hexagonal (sh) $AB_2$ (A = Si; B = Au) structure. The structure of these BSLs is typical of sterically stabilized nanocrystals in this size range and size ratio; however, the thermal decomposition of these BSLs was found to occur by a new and unique pathway. When the BSL is heated above 190 °C, Au nanocrystals coalesce and migrate to the surface of the superlattice while the Si nanocrystals retain a metastable sh superlattice structure.

Si nanocrystals were synthesized by thermal decomposition of hydrogen silsesquioxane, followed by HF etching, thermal hydrosilylation with 1-dodecene, and a final narrowing of the size distribution by solvent/antisolvent size-selective precipitation.[23,24] These nanocrystals have been shown to have a uniform spherical shape and capping ligand coverage.[25] Au nanocrystals were synthesized by gold(III) chloride trihydrate ($HAuCl_4{\cdot}3H_2O$) reduction with sodium borohydride ($NaBH_4$) in the presence of 1-dodecanthiol.[26,27] The nanocrystal size was determined from small-angle X-ray scattering (SAXS) measurements of nanocrystals dispersed in toluene by considering the X-ray scattering intensity expected for a collection of noninteracting nanocrystals of radius $R$[2]

$$I(q) \propto \int_0^\infty N(R)P(qR)R^6\, dR \qquad (1)$$

assuming a Gaussian size distribution $N(R)$, with average radius $\bar{R}$ and standard deviation $\sigma$

**Received:** September 12, 2013
**Accepted:** October 14, 2013
**Published:** October 14, 2013

   dx.doi.org/10.1021/jz401964s | J. Phys. Chem. Lett. 2013, 4, 3677−3682

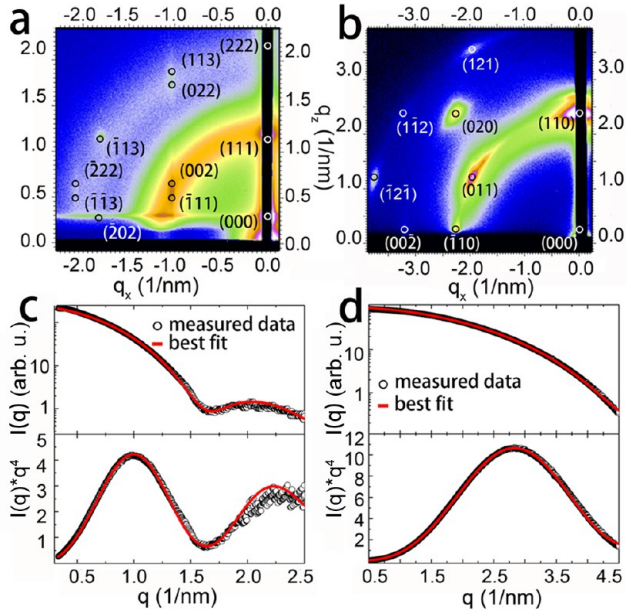


**Figure 1.** GISAXS patterns obtained for superlattices of (a) dodecene-capped Si and (b) dodecanethiol-capped Au nanocrystals used to form BSLs. The diffraction spots index to a (a) fcc superlattice with a lattice constant of $a_{sl,Si}$ = 9.8 nm and a (b) bcc superlattice with lattice constant of $a_{sl,Au}$ = 3.9 nm. (c,d) SAXS data (black circles) for (c) Si and (d) Au nanocrystals dispersed in toluene. The best fits of eqs 1−3 (red lines) to the data gave $\bar{R}$ = 2.70 ($\sigma$ = 0.26 nm) and 0.94 nm ($\sigma$ = 0.10 nm) for the Si and Au nanocrystals, respectively.

$$N(R) = \frac{1}{\sigma\sqrt{2\pi}} \exp\left[\frac{-(R-\bar{R})^2}{2\sigma^2}\right] \quad (2)$$

and using the shape factor for solid homogeneous spheres

$$P(qR) = \left[3\frac{\sin(qR) - qR\cos(qR)}{(qR)^3}\right]^2 \quad (3)$$

The scattering vector is $q = (4\pi/\lambda)\sin(\theta/2)$, where $\lambda$ is the X-ray wavelength and $\theta$ is the scattering angle. Fitting eqs 1−3 to the SAXS data in Figure 1c and d gave average diameters of $d_{core,Si}$ = 5.40 ± 0.53 nm and $d_{core,Au}$ = 1.88 ± 0.19 nm for the Si and Au nanocrystals, respectively. Figure 1a and b shows GISAXS data for superlattices formed with Si or Au nanocrystals. The Si nanocrystal superlattice is fcc with a lattice constant of $a_{sl,Si}$ = 9.8 nm, and the Au nanocrystal superlattice is bcc with a lattice constant $a_{sl,Au}$ = 3.9 nm.

Figure 2 shows TEM images of BSLs formed with the 5.4 nm diameter dodecene-passivated Si nanocrystals and 1.9 nm diameter dodecanethiol-capped Au nanocrystals. (See Supporting Information for the experimental details). The BSL structure is sh-$AB_2$, similar to the intermetallic compound $AlB_2$ with the larger Si nanocrystals creating a sh lattice with smaller Au nanocrystals filling triangular prism interstitial positions. The three different crystallographic projections of the BSLs of $(001)_{bsl}$, $(110)_{bsl}$, and $(100)_{bsl}$ planes viewed down along the lattice directions of $[001]_{bsl}$, $[110]_{bsl}$, and $[210]_{bsl}$, respectively, shown in Figure 2, along with indexing of the fast Fourier transforms (FFTs) of the images are consistent with the sh-$AB_2$ superlattice structure. Figure 3 shows a GISAXS pattern for a BSL of the Si and Au nanocrystals. The pattern exhibits distinct diffraction spots indicating that BSL order is relatively long-range. It indexes to a sh-$AB_2$ structure with lattice constants of $a_{bsl} = b_{bsl}$ = 6.70 nm, $c_{bsl}$ = 6.45 nm, and $\gamma_{bsl}$ = 120°. These dimensions are similar to those determined by TEM, except that the lattice parameter $c_{bsl}$ is slightly contracted by 3.7%. The GISAXS pattern indicates that the superlattice is oriented with $(001)_{bsl}$ planes on the substrate, and therefore, the lattice contraction in the $[001]_{bsl}$ direction occurs *toward the substrate*, most likely as a result of evaporation of solvent retained by the capping ligands after the BSL deposits on the substrate, similar to other evaporated films of BSLs,[13] ordered block copolymers,[28] and mesoporous metal oxides,[29] as illustrated in Figure 3c.

BSL formation was also attempted with larger 6.10 nm diameter Si nanocrystals (9.8% polydispersity) and 1.9 nm diameter Au nanocrystals, but BSL formation was not observed.

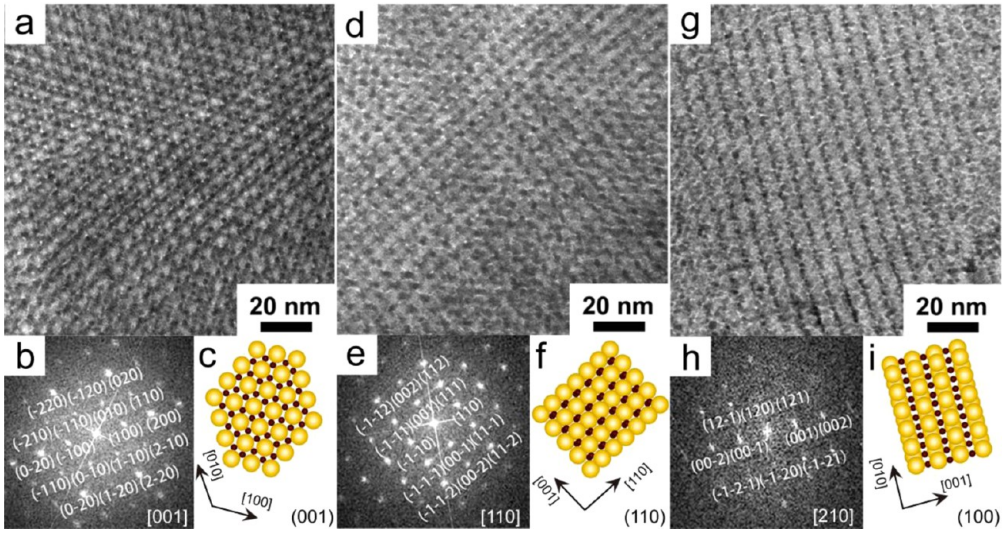


**Figure 2.** TEM images and FFTs of Si/Au BSLs oriented on the grid with different planes: (a,b) $(001)_{bsl}$; (d,e) $(110)_{bsl}$; (g,h) $(100)_{bsl}$. FFTs are indexed to sh-$AB_2$ structure projections, with zone axes in the bottom left corner of each image. (c) Depiction of $(001)_{bsl}$, (f) depiction of $(110)_{bsl}$, and (i) depiction of $(100)_{bsl}$ planes of sh-$AB_2$ BSLs. The *d*-spacings of $(100)_{bsl}$ and $(001)_{bsl}$ superlattice planes are 5.82 and 6.74 nm, corresponding to lattice constants of $a_{bsl}$ = 6.72 nm and $c_{bsl}$ = 6.74 nm.


dx.doi.org/10.1021/jz401964s | J. Phys. Chem. Lett. 2013, 4, 3677−3682

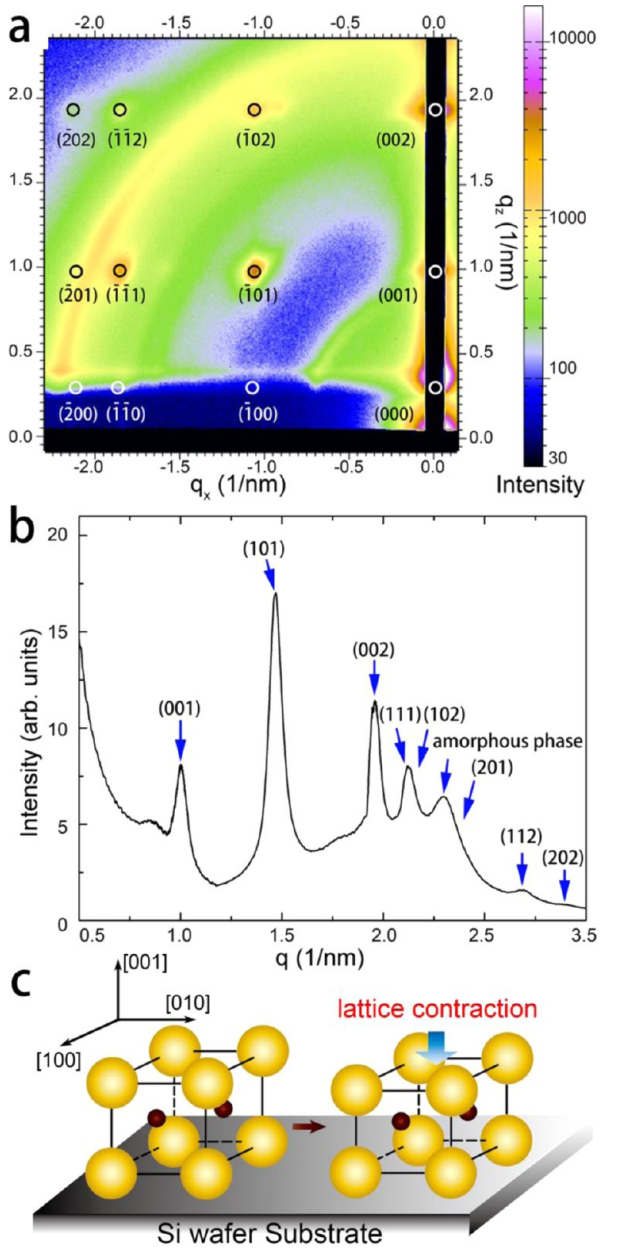


**Figure 3.** (a) GISAXS pattern of a Si/Au BSL. The pattern indexing corresponds to a sh-$AB_2$ structure with lattice constants of $a_{bsl}$ = $b_{bsl}$ = 6.70 nm, $c_{bsl}$ = 6.45 nm, and $\gamma_{bsl}$ = 120°, oriented with the $(001)_{bsl}$ plane on the substrate, which also correspond to a centered orthorhombic (SG 65, *Cmmm*) lattice, with dimensions $a_{bsl}$ = 6.70 nm, $b_{bsl}$ = 11.60 nm, and $c_{bsl}$ = 6.45 nm, oriented with its $(001)_{bsl}$ plane on the substrate. (b) Radial integration of the GISAXS pattern, clearly showing diffraction peaks corresponding to the lattice planes in BSLs. (c) Depiction of the Si/Au sh-$AB_2$ BSL unit cell oriented on the substrate with its $(001)_{bsl}$ plane. The BSL was contracted along its $[001]_{bsl}$ direction toward the substrate.

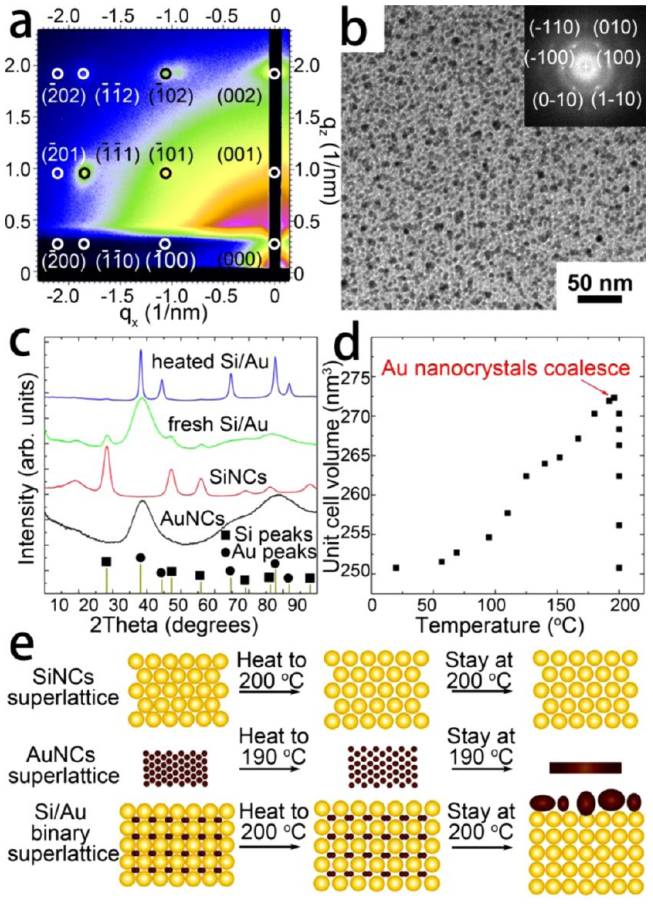


**Figure 4.** (a) GISAXS pattern of the Si/Au BSL that was heated at 200 °C for 10 min. The circles correspond to the simulated spots of the sh superlattice with lattice constants $a_{bsl}$ = $b_{bsl}$ = 6.69 nm, $c_{bsl}$ = 6.45 nm, and $\gamma_{bsl}$ = 120°, oriented on the substrate with its $(001)_{bsl}$ plane. (b) TEM image and FFT of a heated Si/Au BSL oriented on the grid with its $(001)_{bsl}$ plane. (c) XRD of Au nanocrystals, Si nanocrystals, fresh Si/Au BSLs, and heated Si/Au BSLs, showing the coalescence of Au nanocrystals. (d) Plot of the unit cell volume of Si/Au BSLs against temperature, which shows slow lattice expansion due to thermal expansion of capping ligands and fast lattice shrinkage due to the Au nanocrystal coalescence. (e) Depiction of thermal behaviors of Si nanocrystal superlattice, Au nanocrystal superlattice, and Si/Au BSLs.

(See the Supporting Information.) This is perhaps a result of inappropriate size matching. The radius ratio for the 5.4 nm diameter Si nanocrystals and the 1.9 nm diameter Au nanocrystals is nearly ideal for sh-$AB_2$ BSL formation.[13,30] One of the primary driving forces for superlattice formation is space-filling, and entropy encourages the nanocrystals to create the densest structure possible; this is the reason that sterically stabilized nanocrystals tend to form fcc superlattices.[2] The appropriate value to use to check the efficiency of space-filling by the nanocrystals in the structure is the soft sphere radius, which includes some of the capping ligand layer.[2] For instance, in the pure Si and Au nanocrystal superlattices, the center-to-center nearest-neighbor spacings were 6.93 and 3.38 nm, respectively. This includes the diameter of the nondeformable inorganic cores of the nanocrystals and part of the organic ligand shell and represents the soft-sphere diameters of the nanocrystals. The effective thickness of the ligand shell is therefore 0.76 and 0.74 nm for the Si and Au nanocrystals, respectively. Their similar shell thickness is consistent with their similar $C_{12}$ alkyl ligand capping. It should be appreciated that not all of the ligand volume resides in this soft-sphere shell, and the remainder of the ligands fill the rest of the interstitial space in the superlattice.[2] The soft-sphere diameters of the Si and Au nanocrystals in the BSL were determined by first calculating the Si nanocrystal soft-sphere diameter, which is equal to the Si−Si center-to-center nearest-neighbor spacing (i.e., the $(001)_{bsl}$ *d*-spacing of 6.70 nm); then, the Au nanocrystal soft-sphere diameter could be calculated by subtracting this value from the


dx.doi.org/10.1021/jz401964s | *J. Phys. Chem. Lett.* 2013, 4, 3677−3682

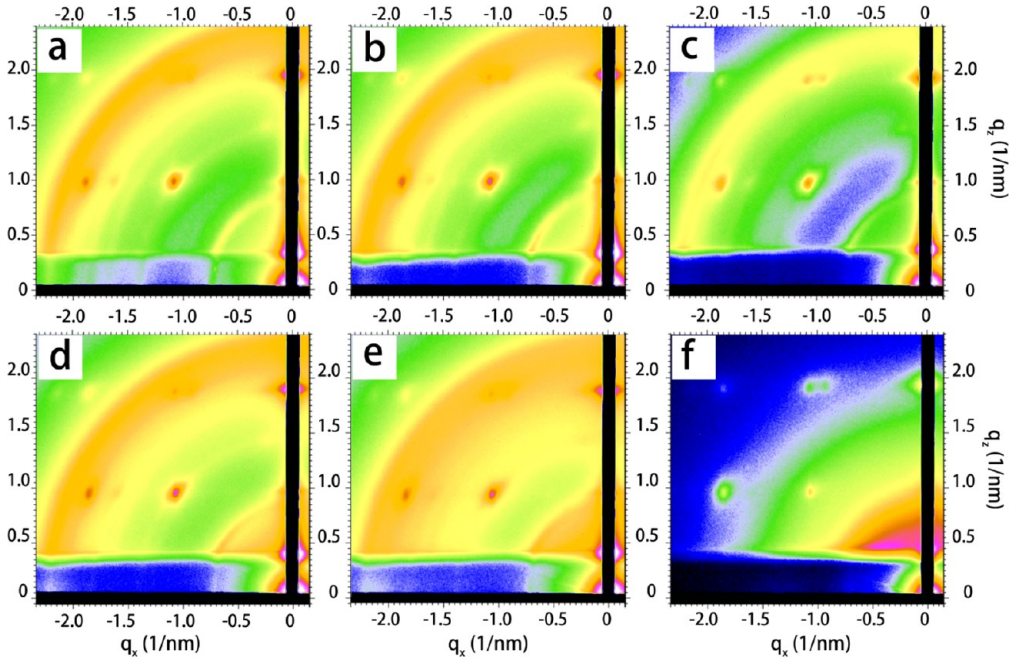


**Figure 5.** GISAXS patterns of a sh-$AB_2$ BSL of Si and Au nanocrystals heated to various temperatures, (a) 20, (b) 50, (c) 95, (d) 152, (e) 199, and (f) after heating at 200 °C for 10 min.

Si–Au center-to-center nearest-neighbor distance of 5.12 nm. The soft-sphere diameter of the Au nanocrystals in the BSL is then 3.53 nm. The (soft-sphere) radius ratio of the Au and Si nanocrystal soft is 0.527, which nearly matches the ideal radius ratio for a sh-$AB_2$ superlattice of 0.528. The ligand shell thicknesses of the Si and Au nanocrystal soft spheres in the BSL of 0.65 and 0.83 nm are also quite close to those in the pure nanocrystal superlattices. It appears that the ligand shell is slightly more compressed for the Si nanocrystals and slightly more expanded for the Au nanocrystals in the BSL.

The thermal stability of the Si–Au BSLs was also studied. Si nanocrystal superlattices are much more stable than Au nanocrystal superlattices at elevated temperature.[23] For instance, superlattices of the Au nanocrystals degrade when heated to 190 °C, whereas the Si nanocrystal superlattices retain their structure when heated to at least 200 °C (see the Supporting Information). Interestingly, when a BSL was heated in air from 20 to 200 °C, the GISAXS pattern (Figure 4a) showed little change, apart from a slight loss in peak intensity. At 200 °C, the pattern indexes to a sh structure with $a_{bsl} = b_{bsl} =$ 6.69 nm, $c_{bsl}$ = 6.45 nm, and $\gamma_{bsl}$ = 120°, with $(001)_{bsl}$ orientation on the substrate. TEM, however, revealed that the Au nanocrystals coalesce when heated above 190 °C; for instance, the Au nanocrystals in the TEM image in Figure 4b of a BSL heated to 200 °C have grown significantly to 8–10 nm in diameter. Still, the underlying Si nanocrystal superlattice is intact, and the Si nanocrystals have not changed size. A FFT of the TEM image in Figure 4b still indexes to a sh lattice with similar dimensions as the initial sh-$AB_2$ BSL. XRD (Figure 4c) also showed that Au nanocrystals in the BSL grow significantly when heated to 200 °C (that is, the Au diffraction peaks sharpen significantly), whereas the Si diffraction peaks remain relatively broad.

When the BSL structure was followed by GISAXS during heating from 20 to 200 °C (Figure 5), an expansion of the lattice was observed (Figure 4d) up to 190 °C. Then abruptly at 200 °C, the superlattice structure contracted significantly. The lattice expansion results from the thermal expansion of the organic ligands.[31,32] The sharp lattice contraction at 200 °C is probably related to migration of the Au nanocrystals from their interstitial positions to the surface of the superlattice, as illustrated in Figure 4e. The surprising result is that despite the loss of Au nanocrystals from the BSL, the sh-Si nanocrystal structure remains intact, despite its low packing density. The reason for the retention of sh structure is probably related to two factors. First, the Si nanocrystals do not coalesce. Unlike the Au nanocrystals, the Si nanocrystals are stable at 200 °C and retain their primary particle size. This might be related to the Si cores, but the ligands are also covalently bonded (Si–C) to the Si surface and do not desorb at this low temperature. The second reason is probably that the energy barrier to transform the sh superlattice into the thermodynamically preferred fcc structure is substantial. Such a superlattice rearrangement requires shifting entire lattice planes by nearly a particle radius (i.e., $R3^{1/2}/2$). The van der Waals attraction between neighboring nanocrystals is too high to overcome in the time frame of the experiment.

In conclusion, Si nanocrystals have been used to form BSLs for the first time. It will be interesting to measure the optical and optoelectronic properties of these Au/Si BSLs. Si nanocrystals, or quantum dots, exhibit bright luminescence that can be tuned by size from visible to near-infrared wavelengths,[24,33,34] but the radiative rate for electron–hole recombination and light emission is typically very slow due to the indirect band gap of Si, usually 10–100 $\mu$s.[35,36] One strategy to enhance the optical properties of Si nanocrystals, or quantum dots, is to position them near a material with a plasmonic optical response, such as Au.[16,37−40] BSLs can provide a unique experimental testbed for examining optical interactions between Si and Au. The Au/Si BSLs also reveal a new approach to creating superlattices with open structures. In this case, a sh superlattice of Si nanocrystals is created by heating the Si/Au BSL to drive the Au out of the lattice. Instead of tuning interparicle interactions and the self-assembly


dx.doi.org/10.1021/jz401964s | J. Phys. Chem. Lett. 2013, 4, 3677–3682

process,[9,11] one of the nanocrystals in the BSL, such as Au nanocrystals in this case, serve as a sacrificial or removable "skeleton" that enables the formation of a metastable open network of nanocrystals, such as the sh superlattice of Si nanocrystals shown here. The Si nanocrystals are rather unique in terms of their thermal stability relative to other sterically stabilized nanocrystals, but this result shows it might be possible to create a variety of metastable superlattice structures by converting BSLs to kinetically trapped structures.

## ■ ASSOCIATED CONTENT

### Supporting Information

Synthesis of Si nanocrystal and Au nanocrystal, experimental details, additional TEM images of BSLs, GISAXS patterns of Au and Si nanocrystal superlattices to 200 °C are included. This material is available free of charge via the Internet at http://pubs.acs.org.

## ■ AUTHOR INFORMATION

### Corresponding Author

*E-mail: korgel@che.utexas.edu.

### Notes

The authors declare no competing financial interest.

## ■ ACKNOWLEDGMENTS

We acknowledge funding of this work by the Robert A. Welch Foundation (Grant No. F-1464) and the National Science Foundation (Grant No. CHE-1308813). CHESS is supported by the NSF & NIH/NIGMS via NSF Award DMR-0936384.

## ■ REFERENCES

(1) Murray, C. B.; Kagan, C. R.; Bawendi, M. G. Self-Organization of CdSe Nanocrystallites into Three-Dimensional Quantum Dot Superlattices. *Science* **1995**, *270*, 1335−1338.
(2) Korgel, B. A.; Fullam, S.; Connolly, S.; Fitzmaurice, D. Assembly and Self-Organization of Silver Nanocrystal Superlattice: Ordered "Soft Spheres". *J. Phys. Chem. B* **1998**, *102*, 8379−8388.
(3) Redl, F. X.; Cho, K.-S.; Murray, C. B.; O'Brien, S. Three-Dimensional Binary Superlattice of Magnetic Nanocrystals and Semiconductor Quantum Dots. *Nature* **2003**, *423*, 968−971.
(4) Shevchenko, E. V.; Talapin, D. V.; Kotov, N. A.; O'Brien, S.; Murray, C. B. Structural Diversity in Binary Nanoparticle Superlattices. *Nature* **2006**, *439*, 55−59.
(5) Doty, R. C.; Bonnecaze, R. T.; Korgel, B. A. Kinetic Bottleneck to the Self-Organization of Bidisperse Hard Disk Monolayers Formed by Random Sequential Adsorption. *Phys. Rev. E* **2002**, *65*, 061503.
(6) Miszta, K.; de Graaf, J.; Bertoni, G.; Dorfs, D.; Brescia, R.; Marras, S.; Ceseracciu, L.; Cingolani, R.; van Roij, R.; Dijkstra, M.; Manna, L. Hierarchical Self-Assembly of Suspended Branched Colloidal Nanocrystals into Superlattice Structures. *Nat. Mater.* **2011**, *10*, 872−876.
(7) Goubet, N.; Richardi, J.; Albouy, P. A.; Pileni, M. P. How to Predict the Growth Mechanism of Supracrystals from Gold Nanocrystals. *J. Phys. Chem. Lett.* **2011**, *2*, 417−422.
(8) Dylla, R. J.; Korgel, B. A. Temporal Organization of Nanocrystal Self-Assembly Directed by a Chemical Oscillator. *ChemPhysChem* **2001**, *1*, 61−64.
(9) Bishop, K. J. M.; Chevalier, N. R.; Grzybowski, B. A. When and Why Like-Sized, Oppositely Charged Particles Assemble into Diamond-like Crystals. *J. Phys. Chem. Lett.* **2013**, *4*, 1507−1511.
(10) Son, J. S.; Lee, J.-S.; Shevchenko, E. V.; Talapin, D. V. Magnet-in-the-Semiconductor Nanomaterials: High Electron Mobility in All-Inorganic Arrays of FePt/CdSe and FePt/CdS Core−Shell Heterostructures. *J. Phys. Chem. Lett.* **2013**, *4*, 1918−1923.
(11) Macfarlane, R. J.; Jones, M. R.; Lee, B.; Auyeung, E.; Mirkin, C. A. Topotactic Interconversion of Nanoparticle Superlattices. *Science* **2013**, *341*, 1222−1225.
(12) Ben-Simon, A.; Eshet, H.; Rabani, E. On the Phase Behavior of Binary Mixtures of Nanoparticles. *ACS Nano* **2013**, *7*, 978−986.
(13) Smith, D. K.; Goodfellow, B.; Smilgies, D.-M.; Korgel, B. A. Self-Assembled Simple Hexagonal $AB_2$ Binary Nanorystal Superlattices: SEM, GISAXS, and Defects. *J. Am. Soc. Chem.* **2009**, *131*, 3281−3290.
(14) Shevchenko, E. V.; Talapin, D. V.; Murray, C. B.; O'Brien, S. Structural Characteriztion of Self-Assembled Multifunctional Binary Nanoparticle Superlattices. *J. Am. Soc. Chem.* **2006**, *128*, 3620−3637.
(15) Saunders, A. E.; Korgel, B. A. Observation of an AB Phase in Bidisperse Nanocrystal Superlattice. *ChemPhysChem* **2005**, *6*, 61−65.
(16) Shevchenko, E. V.; Ringler, M.; Schwemer, A.; Talapin, D. V.; Klar, T. A.; Rogach, A. L.; Feldmann, J.; Alivisatos, A. P. Self-Assembled Binary Superlattices of CdSe and Au Nanocrystals and Their Fluorescence Properties. *J. Am. Soc. Chem.* **2008**, *130*, 3274−3275.
(17) Lu, C.; Chen, Z.; O'Brien, S. Optimized Conditions for the Self-Organization of CdSe−Au and CdSe−CdSe Binary Nanoparticle Superlattices. *Chem. Mater.* **2008**, *20*, 3594−3600.
(18) Evers, W. H.; De Nijs, B.; Filion, L.; Castillo, S.; Dijkstra, M.; Vanmaekelbergh, D. Entropy-Driven Formation of Binary Semiconductor−Nanocrystal Superlattices. *Nano Lett.* **2010**, *10*, 4235−4241.
(19) Lee, D. C.; Smith, D. K.; Heitsch, A. T.; Korgel, B. A. *Annu. Rep. Prog. Chem., Sect. C: Phys. Chem.* **2007**, *103*, 351−402.
(20) Shevchenko, E. V.; Kortright, J.; Talapin, D. V.; Aloni, S.; Alivisatos, A. P. Quasi-Ternary Nanoparticle Superlattices through Nanoparticle Design. *Adv. Mater.* **2007**, *19*, 4183−4188.
(21) Evers, W. H.; Friedrich, H.; Filion, L.; Dijkstra, M.; Vanmaekelbergh, D. Observation of a Ternary Nanocrystal Superlattice and Its Structural Characterization by Electron Tomography. *Angew. Chem., Int. Ed.* **2009**, *48*, 9655−9657.
(22) Dong, A.; Ye, X.; Chen, J.; Murray, C. B. Two-Dimensional Binary and Ternary Nanocrystal Superlattices: The Case of Monolayers and Bilayers. *J. Am. Chem. Soc.* **2011**, *11*, 1804−1809.
(23) Yu, Y.; Bosoy, C. A.; Hessel, C. M.; Smilgies, D.-M.; Korgel, B. A. Silicon Nanocrystal Superlattices. *ChemPhyChem* **2013**, *14*, 84−87.
(24) Hessel, C. M.; Reid, D.; Panthani, M. G.; Rasch, M. R.; Goodfellow, B. G.; Wei, J.; Hiromasa, F.; Akhavan, V.; Korgel, B. A. Synthesis of Ligand-Stabilized Silicon Nanocrystals with Size-Dependent Photoluminescence Spanning Visible to Near-Infrared Wavelengths. *Chem. Mater.* **2012**, *24*, 393−401.
(25) Panthani, M. G.; Hessel, C. M.; Reid, D.; Casillas, G.; Jose-Yacaman, M.; Korgel, B. A. Graphene-Supported High-Resolution TEM and STEM Imaging of Silicon Nanocrystals and Their Capping Ligands. *J. Phys. Chem. C* **2012**, *116*, 22463−22468.
(26) Brust, M.; Walker, M.; Bethell, D.; Schiffrin, D. J.; Whyman, R. Synthesis of Thiol-Derivatised Gold Nanoparticles in a Two-Phase Liquid−Liquid System. *J. Chem. Soc., Chem. Commun.* **1994**, 801−802.
(27) Rasch, M. R.; Rossinyol, E.; Hueso, J. L.; Goodfellow, B. W.; Arbiol, J.; Korgel, B. A. Hydrophobic Gold Nanoparticle Self-Assembly with Phosphatidylcholine Lipid: Membrane-Loaded and Janus Vesicles. *Nano Lett.* **2010**, *10*, 3733−3739.
(28) Bosworth, J. K.; Paik, M. Y.; Ruiz, R.; Schwartz, E. L.; Huang, J. Q.; Ko, A. W.; Smilgies, D. M.; Black, C. T.; Ober, C. K. Control of Self-Assembly of Lithographically Patterned Block Copolymer Films. *ASC Nano* **2008**, *2*, 1396−1402.
(29) Ruland, W.; Smarsly, B. M. Two-Dimensional Small-Angle X-ray Scattering of Self-Assembled Nanocomposite Films with Oriented Arrays of Spheres: Determination of Lattice Type, Preferred Orientation, Deformation and Imperfection. *J. Appl. Crystallogr.* **2007**, *40*, 409−417.
(30) Bodnarchuk, M. I.; Kovalenko, M. V.; Heiss, W.; Talapin, D. V. Energetic and Entropic Contributions to Self-Assembly of Binary Nanocrystal Superlattices: Temperature as the Structure-Directing Factor. *J. Am. Chem. Soc.* **2010**, *132*, 11967−11977.

(31) Korgel, B. A.; Zaccheroni, N.; Fitzmaurice, D. "Melting Transition" of a Quantum Dot Solid: Collective Interactions Influence the Thermally-Induced Order−Disorder Transition of a Silver Nanocrystal Superlattice. *J. Am. Chem. Soc.* **1999**, *121*, 3533−3534.
(32) Korgel, B. A. Correlated Membrane Fluctuations in Nanocrystal Superlattices. *Phys. Rev. Lett.* **2001**, *86*, 127−130.
(33) Hessel, C. M.; Rasch, M. R.; Hueso, J. L.; Goodfellow, B. W.; Akhavan, V. A.; Puvanakrishnan, P.; Tunnel, J. W.; Korgel, B. A. Alkyl Passivation and Amphiphilic Polymer Coating of Silicon Nanocrystals for Diagnostic Imaging. *Small* **2010**, *6*, 2026−2034.
(34) Puzzo, D. P.; Henderson, E. J.; Helander, M. G.; Wang, Z.; Ozin, G. A.; Lu, Z. Visible Colloidal Nanocrystal Silicon Light-Emitting Diode. *Nano Lett.* **2011**, *11*, 1585−1590.
(35) Vial, J. C.; Bsiesy, A.; Gaspard, F.; Hérino, R.; Ligeon, M.; Muller, F.; Romestain, R. Mechanisms of Visible-Light Emission from Electro-Oxidized Porous Silicon. *Phys. Rev. B* **1992**, *45*, 14171−14176.
(36) Mastronardi, M. L.; Maier-Flaig, F.; Faulkner, D.; Henderson, E. J.; Kübel, C.; Lemmer, U.; Ozin, G. A. Size-Dependent Absolute Quantum Yield for Size-Separated Colloidally-Stable Silicon Nanocrystals. *Nano Lett.* **2012**, *12*, 337−342.
(37) Huh, C.; Choi, C.-J.; Kim, W.; Kim, B. K.; Park, B.-J.; Jang, E.-H.; Kim, S.-H.; Sung, G. Y. Enhancement in Light Emission Efficiency of Si Nanocrystal Light-Emitting Diodes by Surface Plasmon Coupling. *Appl. Phys. Lett.* **2012**, *100*, 181108.
(38) Takeda, E.; Nakamura, T.; Fujii, M.; Miura, S.; Hayashi, S. Surface Plasmon Polarity Mediated Photoluminescence from Excitons in Silicon Nanocrystals. *Appl. Phys. Lett.* **2006**, *89*, 101907.
(39) Biteen, J. S.; Pacifici, D.; Lewis, N. S.; Atwater, H. A. Enhanced Radiative Emission Rate and Quantum Efficiency in Coupled Silicon Nanocrystal−Nanostructured Gold Emitters. *Nano Lett.* **2005**, *5*, 1768−1773.
(40) Ratchford, D.; Shafiei, F.; Kim, S.; Gray, S. K.; Li, X. Manipulating Coupling between a Single Semiconductor Quantum Dot and Single Gold Nanoparticle. *Nano Lett.* **2011**, *11*, 1049−1054.